Pattern Formation in Unstable Thin Liquid Films

Ashutosh Sharma* and Rajesh Khanna
Department of Chemical Engineering, Indian Institute of Technology, Kanpur, 208016, India
(Received 20 April 1998)

The problem of spontaneous evolution of morphological patterns in thin (<100 nm) unstable liquid films on homogeneous solid substrates is resolved based on a 3D nonlinear equation of motion. Initially, a small amplitude bicontinuous structure emerges, which either grows and fragments into a collection of microdroplets (for relatively thinner films), or leads directly to isolated circular holes (for thicker films) which dewet the surface. The characteristics of a pattern, and its pathway of evolution, thus depend crucially on the *form* of the intermolecular potential in an extended neighborhood of the initial thickness. The linear and 2D nonlinear analyses used hitherto fail completely in prediction of morphological patterns, but can predict their length scales rather well. [S0031-9007(98)07349-9]

PACS numbers: 68.15.+e, 47.20.Ma, 47.54.+r, 68.45.–v

The problem of stability and spontaneous pattern formation in thin (<100 nm) fluid films is central to a host of technological applications (e.g., coatings) and to a diversity of physical and biological thin film phenomena (e.g., wetting, adhesion, colloids, membrane morphology).

Like all spinodal processes (e.g., phase separation of incompatible materials), the free surface of an initially uniform thin film becomes unstable and deforms spontaneously to engender a microstructure when the second derivative of the excess intermolecular free energy (per unit area) with respect to the (local) film thickness is negative, viz., $\partial^2 \Delta G/\partial h^2 < 0$ [1–4]. Thin film experiments show a variety of microstructures [5–11] ranging from microdroplets to holes, as well as a spectrum of bicontinuous structures. However, our current theoretical understanding of thin film patterns and their relationship to the surface properties/intermolecular interactions is very rudimentary, and even misleading, since it is based largely on the linear stability analysis [1,2], which, e.g., excludes the possibility of circular holes. The 2D nonlinear simulations [3,4] also cannot provide a clue regarding the full 3D morphology of an unstable thin film. The purpose of this Letter is to uncover the variety of morphological patterns which can form spontaneously in an unstable film, and the conditions for the selection of a particular pattern. Complete 3D nonlinear simulations for the first time provide a formalism for correlating the film morphology with the interfacial interactions and the film thickness, and make it possible to directly compare theory and experiments. Among other things, such a formalism will also help address the inverse problem of characterization of surface interactions from the observed morphology.

For simulations, we consider a fairly general excess intermolecular interaction free energy composed of antagonistic (attractive/repulsive) long and (relatively) short range interactions [4,12].

$$\Delta G = -A/12\pi h^2 + S^P \exp(-h/l). \qquad (1)$$

When the van der Waals component of the substrate surface tension exceeds that of the film material, the effective Hamaker constant A is negative [4,12], signifying a long range apolar van der Waals repulsion which promotes film stability and wetting. This is almost always the case for aqueous films and for (relatively) low surface energy polymers on a majority of substrates, e.g., silicon wafers, glass, mica [4,10,12]. The shorter range non-van der Waals attraction ($S^P < 0$) represents the "hydrophobic attraction" [4,10,12] for water ($l \sim 1$–10 nm), as also entropic confinement effects [13] for polymer films due to adsorbed/grafting at the solid-film interface ($l \sim R_g$). Qualitative variations of ΔG and $\partial^2 \Delta G/\partial h^2$ are as shown in Fig. 1. For illustration, a realistic set of parameters are chosen, but based on a large number of simulations, we have verified that all of the key morphological features (e.g., whether a circular hole forms) depend on the *form* of potential, rather than its magnitude. Finally, the *form* of potential in the complementary case of a long range attraction combined with a strong shorter range repulsion is a special case of potential shown in Fig. 1, when the correlation length l is considered to be large and, thus, the unstable spinodal region ($h < h_c$ where $\partial^2 \Delta G/\partial h^2 < 0$) formally extends to infinity (viz., $h_c \to \infty$, instead of about 17 nm as in Fig. 1).

The following nondimensional thin film equation [14], derived from the Navier-Stokes equations, governs the

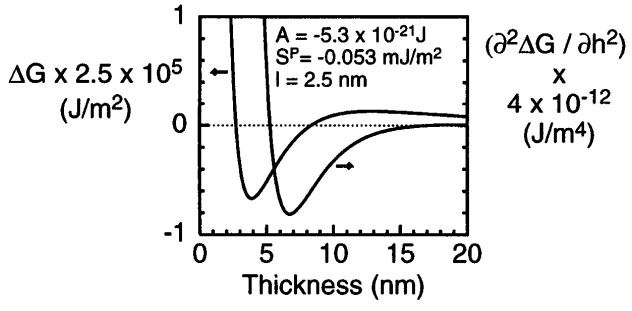

FIG. 1. Variations of the free energy per unit area, ΔG, and force per unit volume, $\partial^2 \Delta G/\partial h^2$, with film thickness. Instability occurs for $5.3 < h < 17$ nm, where $\partial^2 \Delta G/\partial h^2 < 0$.

stability and spatiotemporal evolution of a thin film subjected to the excess intermolecular interactions (where $\Phi_H = [2\pi h^2/|A|][\partial^2 \Delta G/\partial H^2]$).

$$\partial H/\partial T + \nabla \cdot [H^3 \nabla(\nabla^2 H)] - \nabla \cdot [H^3 \Phi_H \nabla H] = 0, \quad (2)$$

where H (X, Y, T) is the nondimensional local film thickness scaled with the mean thickness, h; X, Y coordinates in the plane of substrate are scaled with the characteristic length scale for the van der Waals case [4], $(2\pi\gamma/|A|)^{1/2} h^2$; and nondimensional time T is scaled with $(12\pi^2 \mu\gamma h^5/A^2)$; where γ and μ refer to film surface tension and viscosity. A renormalized real time, $t_N = t(A^2/12\pi^2\mu\gamma) = Th^5$ can also be defined to remove the influence of mean film thickness.

The second term of the thin film equation denotes the effect of surface tension for a curved surface, which in a 3D geometry may be stabilizing (due to "in-plane" curvature as in 2D cases) or destabilizing (due to transverse curvature as in Raleigh instability of circular cylinders). The third term describes the effect of excess intermolecular interactions, which engender instability by causing flow from thinner to thicker regions in the case of negative "diffusivity," viz., when $\Phi_H < 0$.

The linear stability analysis [1,14] of the 3D thin film Eq. (2) predicts a dominant characteristic length scale of the instability, $\lambda = 4\pi/\sqrt{-\Phi_H}$, which is the diagonal length of a unit square cell of length $L = \lambda/\sqrt{2}$. In order to address the problem of pattern selection, we directly solved the nonlinear thin film equation numerically over an area of nL^2 ($n = 4$ or 16), starting with an initial small amplitude ($\approx$1 Å) random perturbation. A 30×30 grid ($n = 4$) and a 60×60 grid ($n = 16$) were found sufficient when central differencing in space with half node interpolation was combined with Gear's algorithm for time marching, which is especially suitable for stiff equations.

We found two completely different morphological patterns and their sequence of evolution by which (pseudo-) dewetting can occur, depending on the *form* of the potential in the neighborhood of the initial film thickness. Figure 2 summarizes the major events in the time evolution of patterns in a relatively thick 16 nm film (close to the critical thickness), which is sufficiently removed from the location of the minimum in the free energy where repulsion becomes important (Fig. 1). The initial random disturbance is first reorganized into a small amplitude bicontinuous pattern on a length scale close to λ. This stage is reminiscent of the linear concentration field in the spinodal decomposition [1]. Long "hills" of the structure undergo some fragmentation, while the "valleys" thin locally to produce largely *circular full thickness* holes surrounded by circular uneven (in height) rims. As expected [4] a true dewetting of the substrate, however, does not occur at the base of these holes (white areas), where a nearly flat film of thickness close to the location of the

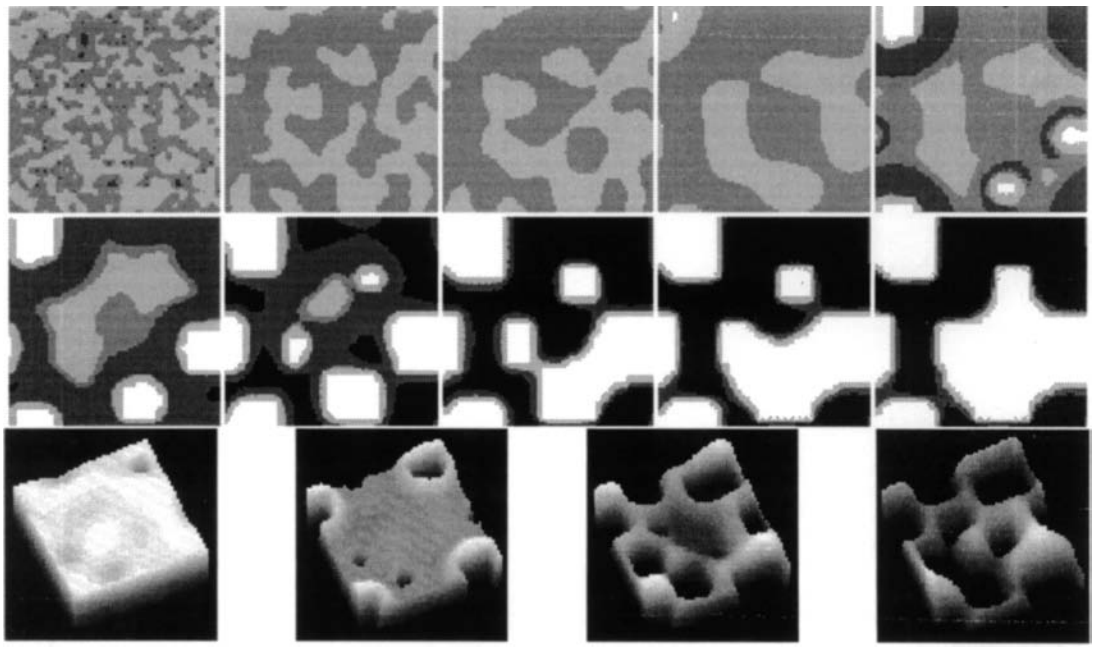

FIG. 2. Different stages of evolution of a pattern in a 16 nm thick film. Gray scale pictures in the first two rows correspond to (from left to right) $T = 0$, 1, 7, 110, 131, 144, 167, 260, 460, and 6000, respectively. Area of each cell is $4L^2$ and increasing shades of gray (from white to black) represent nondimensional thickness H in the range of 0.25 (equilibrium thickness) $< 0.4 < 1 < 1.07 < 1.5 < 3.64$ (maximum thickness). Complete 3D morphology is shown over an area of $6.25L^2$ in the third row at $T = 110$, 130, 161, and 260. The maximum and minimum thicknesses (in nm) in the 3D pictures are (17, 4), (22, 4), (31, 4), and (45, 4).

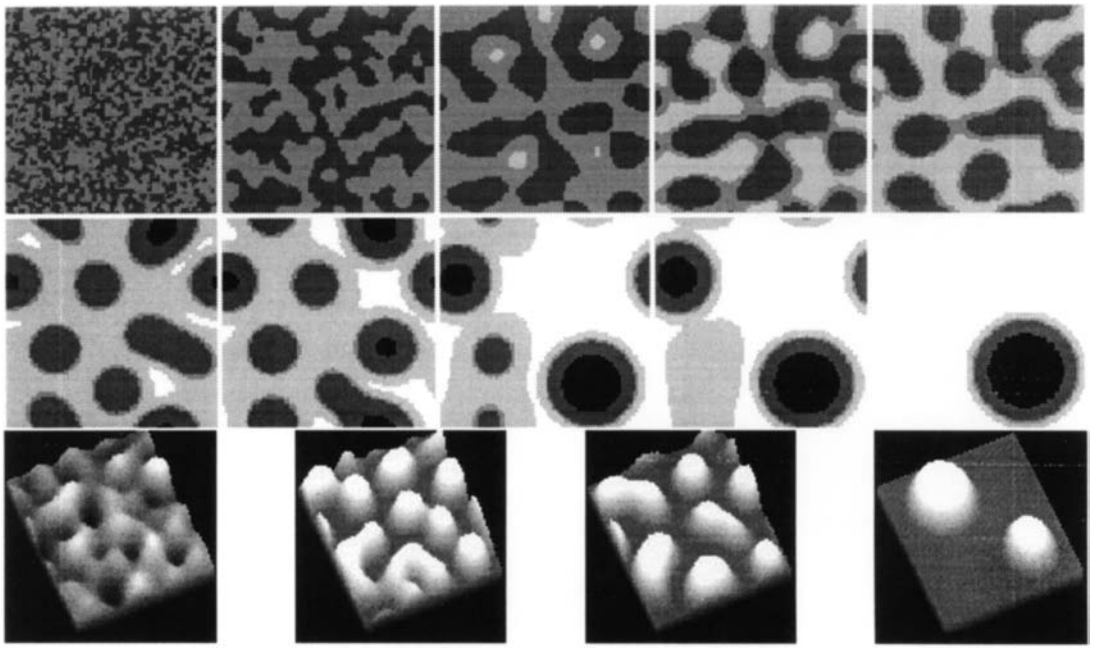

FIG. 3. Different stages of evolution of pattern in a 7 nm thick film over an area of $16L^2$. Gray scale pictures correspond to (from left to right) $T = 0$, 0.6, 56, 77, 100, 155, 237, 1334, 1713, and 20000, respectively. The gray scale is (from white to black) 0.58 (equilibrium thickness) $< 0.6 < 0.8 < 1 < 2.4 < 4.12$ (maximum). 3D morphologies in the third row are shown at $T = 10$, 100, 134, and 1713. In 3D pictures, maximum and minimum thickness (in nm) are (7.5, 6.6), (14, 4), (18, 4), and (26, 4).

expand by the displacement of their (pseudo-) contact lines. Eventually, a repeated coalescence of holes suggests rudiments of a polygonal structure in which the intervening pools of liquid slowly fragment and transform into increasingly circular droplets (long time results not shown). Interestingly, a very similar sequence of morphological evolution (bicontinuous pattern → circular holes with rims → hole expansion → hole coalescence) was also shown [14] by simulations for *all thicknesses* in thin films subjected to only a long range van der Waals *attraction.* This indicates a rather general pathway of pattern evolution and dewetting by the formation of full thickness, isolated holes (viz., air-in-liquid dispersion) whenever the initial mean thickness (viz., liquid phase concentration) is sufficiently high so that the repulsive interactions at the minimum thickness are encountered only after a considerable growth of the instability. The formation of circular holes is therefore not *necessarily* indicative of "nucleation" by large dust particles, defects, etc. [9], but can *also* occur by a spontaneous growth of surface instability. This explains the experiments of Thiele *et al.* [10], who observed the formation of circular holes by spinodal mechanism in evaporating aqueous films [the form of their potential is identical to Eq. (1); Fig. 1], since the instability of initially thick evaporating films is initiated close to the critical thickness.

In contrast to the above scenario, Fig. 3 depicts a different universal pathway of evolution for relatively thin ($<$8 nm in Fig. 1) unstable films which encounter repulsion in the early stages of growth. A bicontinuous structure composed of long hills and valleys persists (without the formation of circular holes) until the fragmentation of "hills" directly produces an array of microdroplets (viz., liquid-in-air dispersion). These droplets become increasingly circular due to surface tension and increase in height due to flow from the "valleys" which thin and flatten out. The formation of flat equilibrium film (pseudo-contact line) occurs *after* the formation of isolated droplets. Thus, in this case, the (pseudo-) dewetting occurs by retraction of droplets, rather than by the expansion of holes. At long times, ripening of the structure continues by the merger of neighboring droplets due to the Laplace pressure induced flow from the smaller to bigger drops. Eventually, a truly thermodynamic stable state is reached, which is represented by the coexistence of a single drop with its surrounding equilibrium flat thin film or "pseudo-partial wetting." The same qualitative pathway of morphological evolution was seen in a large number of simulations (not shown) for all thicknesses to the left of the minimum in the $\partial^2 \Delta G/\partial h^2$ curve, and thicknesses close to the right of it, regardless of the numerical values of the parameters A, S^P, and l which characterize the potential.

Thus, it is the *form* of the potential which governs vastly different morphological patterns and their sequence of evolution (i.e., isolated holes leading to pseudodewetting *before* droplets are formed, or large amplitude bicontinuous ridges leading to dewetting by droplets). Therefore, on a chemically (or physically) heterogeneous substrate, both types of pattern can coexist. While the *form* of the potential selects the morphology, it is the precise *magnitude* of $\partial^2 \Delta G/\partial h^2$ which determines the actual (dimensional) characteristic length scale

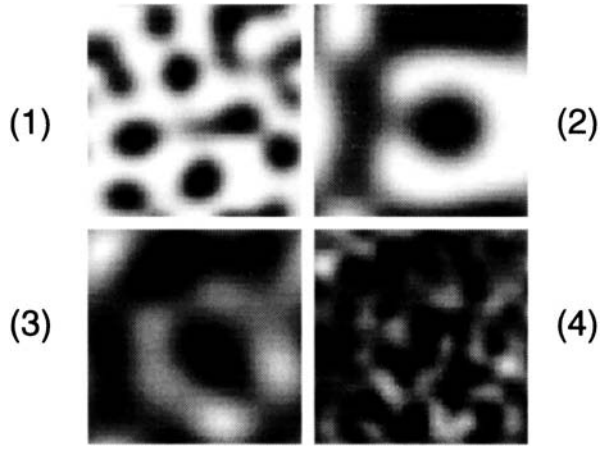

FIG. 4. Gray scale images of 7, 9, 13, and 16 nm thick films (pictures 1 to 4, respectively) at the same renormalized real time, $t_N = 1.9 \times 10^6$ nm^5. Areas shown are $4L^2$ except for picture 1, where it is $16L^2$. A continuous linear gray scale between the minimum and the maximum thickness in each picture is used.

of the pattern, as implied by Eq. (2) and its linear analysis. Also, a large number of simulations showed that about three to five drops (or holes) are initially formed on a substrate area of $4L^2$, which also confirms the expectation of the linear theory, *before* a significant ripening of drops or hole coalescence occurs. Thus, although the linear theory can be used as a good approximation for prediction of length scales (or for the prediction of the potential, $-\Phi_H = 16\pi^2/\lambda^2$ from the observed λ), it fails completely in prediction of the morphological patterns (holes, bicontinuous ridges, drops, etc).

For a range of intermediate thickness (8–10 nm in Fig. 1), the initial bicontinuous pattern resolves into a mixture of both drops *and* (partial thickness) holes in varying proportions, depending on the distance from the minimum in the potential (simulations not shown). An increase in the film thickness from Fig. 3 increases the relative population of isolated circular depressions of increasing depth and increasingly well-formed rims, until the mature, full thickness holes shown in Fig. 2 are obtained at higher thicknesses (about 11 nm). Conceptually, this phenomenon (droplets-in-air → holes-in-liquid) can be thought of as a transient "morphological phase-inversion" in which liquid film thickness, which is an analog of concentration, is the control parameter.

Different pathways and kinetics of pattern evolution can produce strikingly different morphologies at the same real time in different thickness films, as shown for comparison in Fig. 4. Because of a faster evolution of instability in thinner films, formation of droplets in a 7 nm film is already visible at the time when the initial phase of evolution is proceeding in a 16 nm film, which will eventually result in expanding circular holes. Very similar morphologies have been experimentally observed previously (Fig. 2 of Zhao *et al.* [6]) and in recent experiments with PDMS films [9]. Detailed comparisons will be published elsewhere.

An important conclusion is that different morphologies (isolated circular holes, droplets, bicontinuous) and their combinations can all be produced by the *spinodal decomposition mechanism* depending on the film thickness *vis-a-vis* the location of the minimum in the spinodal parameter. Moreover, all of the three patterns (holes and drops of varying sizes, bicontinuous ridges, droplets) can coexist at a given time, most prominently, on heterogeneous surfaces. This should help in correct interpretation of thin film experiments, where, in the absence of 3D nonlinear results, the linear analysis has widely been used as a guide. Most notably, the latter excludes the possibility of circular holes and their sequential formation. There is also a way now to correlate the *quantitative* aspects of morphological patterns in thin films with the excess intermolecular forces and the film thickness by a quantitative matching of patterns.

We thank Gunter Reiter for very useful discussions and suggestions. This work was supported by a grant from the Indo-French Centre for the Promotion of Advanced Research/Centre Franco-Indien Pour la Promotion de la Recherche.

Note added in proof.—A recent publication [R. Xie *et al.*, Phys. Rev. Lett. **81**, 1251 (1998)] has reported dewetting by the formation of droplets in thin polystyrene films similar to the pathway shown in Fig. 3.

*Corresponding author.

[1] A. Vrij, Discuss. Faraday Soc. **42**, 23 (1966).
[2] E. Ruckenstein and R. K. Jain, J. Chem. Soc. Faraday Trans. 2 **70**, 132 (1974).
[3] M. B. Williams and S. H. Davis, J. Colloid Interface Sci. **90**, 220 (1982).
[4] A. Sharma, Langmuir **9**, 861 (1993); A. Sharma and A. T. Jameel, J. Colloid Interface Sci. **161**, 190 (1993).
[5] G. Reiter, Phys. Rev. Lett. **68**, 75 (1992); Langmuir **9**, 1344 (1993); G. Reiter, P. Auroy, and L. Auvray, Macromol. **29**, 2150 (1996).
[6] W. Zhao *et al.*, Phys. Rev. Lett. **70**, 1453 (1993).
[7] J. M. Guerra, M. Srinivasrao, and R. S. Stein, Science **262**, 1395 (1993).
[8] L. Sung, A. Karim, J. F. Douglas, and C. C. Han, Phys. Rev. Lett. **76**, 4368 (1996).
[9] J. Bischof, D. Scherer, S. Herminghaus, and P. Leiderer, Phys. Rev. Lett. **77**, 1536 (1996).
[10] U. Thiele, M. Mertig, and W. Pompe, Phys. Rev. Lett. **80**, 2869 (1998).
[11] G. Reiter *et al.* (to be published).
[12] C. J. van Oss, M. K. Chaudhury, and R. J. Good, Chem. Rev. **88**, 927 (1988); J. N. Israelachvili, *Intermolecular and Surface Forces* (Academic Press, London, 1992).
[13] K. R. Shull, J. Chem. Phys. **94**, 5723 (1991); Faraday Discuss. **98**, 203 (1994).
[14] R. Khanna and A. Sharma, J. Colloid Interface Sci. **195**, 42 (1997).